Synthesis and Optical Characterization of Lead-Free Phenylenediammonium Bismuth Halide Perovskites: A Long Charge Carrier Lifetime in Phenylenediammonium Bismuth Iodide

Zumaira Siddique,[1,2,3] Julia L. Payne,[3*] Muhammad T. Sajjad,[4,5] Natalie Mica,[4] David B. Cordes,[3] Alexandra M. Z. Slawin,[3] Ifor D. W. Samuel,[4] Azhar Iqbal,[1*] John T. S. Irvine[3*]

[1]Department of Chemistry, Quaid-i-Azam University, Islamabad, 45320, Pakistan.

[2]Department of Chemistry, Government College University, Jhang Road, Faisalabad, 38000, Pakistan.

[3]EaStCHEM School of Chemistry, University of St Andrews, North Haugh, St Andrews, KY16 9ST, United Kingdom.

[4]Organic Semiconductor Centre, SUPA, School of Physics and Astronomy, University of St Andrews, North Haugh, St Andrews, KY16 9SS, United Kingdom.

[5]London Centre for Energy Engineering, School of Engineering, London South Bank University, 103 Borough Road, London, SE1 0AA, United Kingdom.

Correspondence should be addressed to Dr Julia L. Payne, jlp8@st-andrews.ac.uk, Dr Azhar Iqbal, aiqbal@qau.edu.pk or Prof. John T.S. Irvine, jtsi@st-andrews.ac.uk.

Abstract:

Toxicity and regulatory concerns over the use of $(CH_3NH_3)PbI_3$ in photovoltaic devices have resulted in significant interest in lead-free, organic-inorganic metal halides with excellent light absorbing properties and stability. Here we report the synthesis of three new lead-free bismuth halides which accommodate the symmetric conjugated *p*-phenylenediammonium

cation (PPD = $(H_3NC_6H_4NH_3)^{2+}$) in the structures. These are (PPD)BiI_5, (PPD)$[BiBr_4]_2 \cdot 2H_2O$ (**2**) and (PPD)$_2BiCl_7 \cdot H_2O$. We also synthesized β-(PPD)$_2Bi_2I_{10}$. The band gap of the iodide, β-(PPD)$_2Bi_2I_{10}$ (1.83 eV) is lower than that of the bromide, (PPD)$[BiBr_4]_2 \cdot 2H_2O$ (2.64 eV) and chloride, (PPD)$_2BiCl_7 \cdot H_2O$ (2.93 eV). Photophysical studies show that β-(PPD)$_2Bi_2I_{10}$ has the longest average charge carrier lifetime (>1 μs) of the materials studied here, of the same order of magnitude as that of $(CH_3NH_3)PbI_3$ and has a low band gap. This suggests that β-(PPD)$_2Bi_2I_{10}$ may be a promising candidate for use in lead-free photovoltaic devices.

Key Words:

$(H_3NC_6H_4NH_3)^{2+}$ cation; aromatic; hybrid perovskite; 1D; time resolved photoluminescence; 0D; single crystal; photovoltaics.

1. Introduction

Increasing energy consumption and the shortage of fossil fuels are forcing the scientific community to search for new solutions to fulfil energy demands. More than 15 TW energy per year is consumed by the world's population and this is predicted to increase to 30 TW in 2050. [1] In one year, the sun can provide 1.7×10^5 TW of energy, which is more than enough to fulfill the energy demands of the whole planet, if a small proportion of this energy could be harnessed.[2] For many years, photoelectrochemical and photovoltaic devices have been developed to convert sunlight into electrical energy.[3] Following the development of first generation single crystalline silicon solar cells and polycrystalline thin film second generation solar cells, scientists are now focusing on low cost, economical and efficient solar cell materials.[4] One notable development was the replacement of organic dyes in dye-sensitized solar cells with hybrid perovskite materials based on $(CH_3NH_3)PbI_3$, which resulted in significant increases in power conversion efficiencies. The term 'hybrid' arises due to the materials containing both an inorganic and organic component. Since 2009, when the use of

$CH_3NH_3PbI_3$ in a photovoltaic device was first reported, the efficiency of these perovskite based devices has increased from 3.8 % to 25.5%.[5] High absorption coefficients, long charge carrier diffusion lengths, high carrier mobilities, tunable band gaps, weak exciton binding energies and low non-radiative recombination rates make these hybrid perovskites excellent candidates for a variety of photovoltaic applications.[6] The diversity of atomic compositions, low temperature device processing methods and device architectures have resulted in the development of cheap and effective photovoltaic devices.[7] Despite these benefits, the two main drawbacks of $(CH_3NH_3)PbI_3$ are the toxicity of lead and the instability of $(CH_3NH_3)PbI_3$ under ambient conditions, which hinder their commercialization.[8]

Other metal cations such as tin (II), germanium (II) and bismuth (III) have been explored as alternatives to lead in halide perovskites.[9-11] Bismuth (III) based hybrid perovskites have been widely used as a result of their lower toxicity, high absorption coefficients, iso-electronicity to Pb^{2+} ($6s^2$, $6p^0$) and low oxidation in solution.[12] Solution processable hybrid bismuth (III) based halides can form a range of different structure types, where bismuth iodide octahedra may exist in the form of isolated zero dimensional octahedra,[13, 14] one dimensional interconnected chains of octahedra,[15] two dimensional layers of octahedra or chains that extend in two directions,[16-19] and three dimensional networks of octahedra.[20] The connectivity of these octahedra could be through face, edge or corner sharing.[21] Due to the greater choice and flexibility in organic cations, unique structural and optoelectronic properties can be linked with one dimensional (1D), 2D and quasi-2D layered materials.[22] So, by choosing versatile fabrication methodologies, exploring new materials and testing different device architectures, these materials should be capable of being fabricated at the industrial scale with the improved stability and performance that are required for commercialization.[23]

There are several examples of phenylenediammonium metal halides reported in the literature.[24-27] In addition, organic cations that are closely related to phenylenediammonium

have also been used in the preparation of organic-inorganic metal halides.[28] However, many of these studies focus on the crystallography rather than the properties of these materials. The structure of *p*-pheneylenediammonium (PPD) bismuth iodides (and a corresponding hydrate) and a *p*-phenylenediammonium bismuth chloride have previously been reported.[24-27] $PPDBi_2I_8 \cdot I_2$ consists of chains of edge sharing BiI_6 octahedra and also contains molecules of I_2, which form a pseudo-3-dimensional structure due to the short intermolecular I-I distances between iodine in the I_2 molecules and the BiI_6 octahedra.[27] $PPDBi_2I_8 \cdot I_2$ is stable up to temperatures of 100 °C and has a low band gap of 1.45 eV, although further properties of the compound are currently unexplored.[27] $PPD_2Bi_2I_{10}$ exists in two polymorphs, α and β, with the α-β phase transition occurring at -26 to -28 °C.[24] Both α and β-$PPD_2Bi_2I_{10}$ consist of isolated, edge sharing Bi_2I_{10} dimers. In addition, the reported structure of the hydrate, $PPD_2Bi_2I_{10} \bullet 4H_2O$ is very similar to the published β-$PPD_2Bi_2I_{10}$ and again consists of Bi_2I_{10} dimers.[24, 25] There is also one report of a *p*-phenylenediammonium bismuth chloride, $PPD_2BiCl_7 \cdot H_2O$, in the literature which consists of isolated $BiCl_6$ octahedra.[26] A peak in differential scanning calorimetry data along with a change in the dielectric constant of $PPD_2BiCl_7 \cdot H_2O$, both at 90 °C, provide evidence for a phase transition.[26] It is thought that this phase transition relates to an order-disorder transition, probably driven by the reorganization of water or PPD molecules.[26] Despite the improvement in optoelectronic properties by lowering non-radiative recombination in low dimensional materials, and enhanced moisture stability in organic metal halides containing aromatic amines, few studies have explored the use of symmetric conjugated amines, which are more compact and form rigid structural configurations with metal halides.[29] Therefore, the aim of this work was to probe the synthesis, structural characterization and optoelectronic properties of *p*-phenylenediammonium bismuth halide materials. Compounds of this type may also have possible applications in ferroelectrics, lasers, light emitting diodes (LEDs), solar cells or super lattice heterojunction devices.[30-32]

2. Experimental

2.1. Materials

p-Phenylenediamine ($H_2NC_6H_4NH_2$, 97%, Alfa Aesar), bismuth(III) oxide (Bi_2O_3, 99.975%, Alpha Aesar), hypophosphorous acid solution (H_3PO_2, 50 wt % H_2O, Sigma Aldrich), hydriodic acid (HI, 57 % w/w aqueous solution, stabilized with 1.5 % hypophosphorous acid, Alfa Aesar), hydrobromic acid (HBr, 48 % w/w aqueous solution, Alfa Aesar), hydrochloric acid (HCl, 37 % w/w aqueous solution, Fisher Chemical), absolute ethanol (C_2H_5OH, VWR BDH Chemicals), and diethyl ether ($C_4H_{10}O$, 99.5%, Riedel-de Haen) were used as received unless otherwise specified.

The *p*-phenylenediamine dihydriodide salt (PPD2HI) was prepared by the stoichiometric reaction of *p*-phenylenediamine with hydriodic acid. The *p*-phenylenediamine was dissolved in in 20 mL ethanol and HI was added dropwise to the solution in a round bottom flask at 0 °C to adjust the pH to around 6-7. The mixture was stirred for two hours, then the solvent was removed using a rotary evaporator at 80 °C. The crude yellowish-white powder was recrystallised three times from ethanol and diethyl ether. Afterwards the white product was filtered and dried at 70 °C in vacuum oven overnight. The equivalent procedure was followed for the synthesis of *p*-phenylenediamine dihydrobromide (PPD2·HBr) and *p*-phenylenediamine dihydrochloride salts (PPD·2HCl) by using HBr and HCl precursors instead of HI.

2.2. Synthesis of $(PPD)BiI_5$ and β-$(PPD)_2Bi_2I_{10}$

Bismuth (III) oxide was dissolved in a mixture of hydriodic acid (HI, 10 mL) and hypophosphorous acid (HPA, 2mL) at 180 °C for 10 minutes with constant stirring. A dark red precipitate was immediately formed upon the addition of PPD·2HI (3.64 g, 10 mmol) salt to this hot solution. By changing the ratio of reactants, two different types of bismuth iodide materials were formed. To prepare compound $(PPD)BiI_5$, a 1:1 ratio is used (4.66 g, 10 mmol

Bi_2O_3 and 3.64 g, 10 mmol PPD2HI), whereas to prepare β-$(PPD)_2Bi_2I_{10}$ a 1:2 ratio is used (2.33 g, 5 mmol Bi_2O_3 and 3.64 g, 10 mmol PPD2HI). This non-stoichiometric ratio of organic cation to metal halide has previously been used in the synthesis of other hybrid perovskites containing diamines, enabling the desired product to be grown from the solution.[33]

To prepare phase pure crystalline β-$(PPD)_2Bi_2I_{10}$, stirring was discontinued after 20 minutes and the solution was cooled down to room temperature over 48 hours, which allowed the crystals to grow. After that, the crystals were filtered and dried at 70 °C in a vacuum oven for 24 hours. The atomic % (found / calculated) of Bi (17.76 / 16.67) and I (82.24/ 83.33) from EDX analysis of crystals confirmed the Bi:I ratio in this sample**.** This compound matches the previously described compound β-$PPD_2Bi_2I_{10}$.[24]

2.3. Synthesis of $(PPD)[BiBr_4]_2 \cdot 2H_2O$

Bismuth (III) oxide (2.33 g, 5 mmol) was dissolved in a mixture of hydrobromic acid (HBr, 10 mL) and hypophosphorous acid (HPA, 2mL) at 180 °C for 10 minutes with constant stirring. A light green precipitate was formed upon the subsequent addition of PPD·2HBr salt (2.70 g, 10 mmol) to this hot solution. For the growth of crystals, the stirring was discontinued after 20 minutes and the solution was cooled to room temperature over 48 hours. After that, the crystals were filtered and dried in a vacuum oven at 70 °C for 24 hours. Powder X-ray diffraction showed that $(PPD)[BiBr_4]_2 \cdot 2H_2O$ was the major phase present, with a small amount of the bromide equivalent of β-$PPD_2Bi_2I_{10}$ (*i.e.* β-$PPD_2Bi_2Br_{10}$) present as an impurity phase (see supporting information). The atomic % (found / calculated) of Bi (18.26/ 16.67) and Br (81.74/ 83.33) from EDX analysis of crystals confirmed the Bi:Br ratio.

2.4. Synthesis of $(PPD)_2BiCl_7 \cdot H_2O$

Bismuth (III) oxide (2.33 g, 5 mmol) was dissolved in a mixture of hydrochloric acid (HCl, 10 mL) and hypophosphorous acid (HPA, 2 mL) at 180 °C for 10 minutes with constant stirring. A colourless precipitate was formed upon the addition of PPD·2HCl salt (1.81 g, 10

mmol) to this hot solution. For the growth of crystals, the stirring was discontinued after 20 minutes and the solution was cooled to room temperature over 48 hours. Afterwards the crystals were filtered and dried in a vacuum oven at 70 °C for 24 hours. Powder X-ray diffraction and EDX analysis confirmed the phase purity of $(PPD)_2BiCl_7{\cdot}2H_2O$. The atomic % (found / calculated) of Bi (16.57/ 16.67) and Cl (83.43/ 83.33) from EDX analysis of crystals confirmed the Bi:Cl ratio.

Images of the samples of β-$(PPD)_2Bi_2I_{10}$, $(PPD)[BiBr_4]_2{\cdot}2H_2O$ and $(PPD)_2BiCl_7{\cdot}H_2O$ are shown in Figure S1.

2.5. Physiochemical Techniques

UV-Visible absorption spectra of the powdered samples were measured using a V650 spectrophotometer (Jasco) with $BaSO_4$ as a reference. The room temperature steady-state and time-resolved photoluminescence (PL) of thin films of samples on quartz substrates were performed using an Edinburgh Instruments FLS980 spectrometer. For PL lifetime measurements, samples were excited at 379 nm by a PicoQuant picosecond pulsed laser (PicoQuant, LDH-D-C-375) and PL was detected using a time correlated single photon counting (TCSPC) setup. Powder X-ray diffraction data were collected using a Panalytical Empyrean X-ray diffractometer operating in Bragg-Brentano geometry with $CuK\alpha_1$ radiation and an X'celerator RTMS detector. Data were collected in the range 5-70° 2θ, with a step size of 0.017° and a time per step of 0.94 s. Single crystal X-ray diffraction data were collected at 173 K using a Rigaku FR-X Ultrahigh Brilliance Microfocus RA generator/confocal optics with Rigaku XtaLAB P200 diffractometer [Mo Kα radiation (λ = 0.71075 Å)]. Intensity data were collected using ω steps accumulating area detector images spanning at least a hemisphere of reciprocal space. Data for all compounds were collected using CrystalClear and processed using either CrystalClear[34] or CrysAlisPro.[35] Structure solution was carried out by dual-space methods using SHELXT[36] and structure refinement by full matrix least squares against F^2 was

carried out with SHELXL (2014/7).[37] Non-hydrogen atoms were refined anisotropically and aromatic hydrogen atoms were refined using a riding model. Amine hydrogens were located from the difference Fourier map and refined isotropically subject to a distance restraint. All calculations were performed using the WinGX interface.[38] Selected crystallographic data are presented in Tables 1 and S1. Deposition numbers 2180531–2180533 contains the supplementary crystallographic data for this paper. These data are provided free of charge by the joint Cambridge Crystallographic Data Centre and Fachinformationszentrum Karlsruhe Access Structures service: www.ccdc.cam.ac.uk/structures. SEM images and EDS (Figure S7) were taken on a Jeol 6700 F microscope. FTIR spectra were obtained using an IR Infinity spectrometer in the range of 400-4000 cm^{-1}.

3. Results and Discussion

3.1 Crystal Structure Analysis

The structure of (PPD)BiI_5 was determined from single crystal XRD data and is shown in Figure 1. It crystallizes in the space group $P2_1$ and consists of one-dimensional chains of corner sharing BiI_6 octahedra, which run along the *b*-axis in a zig-zag motif. These chains are separated by PPD cations. Similar chains have been observed in other materials such as N-3-aminopropylimidazolium lead iodide.[39] The asymmetric unit comprises of a bismuth atom, five symmetrically inequivalent iodine atoms and a PPD molecule. The Bi-I bond lengths range from 2.9055(6) Å to 3.3504(6) Å (Table 2), with I-Bi-I bond angles ranging from 83.387(8)° to 98.522(17)°. The bismuth atom is off-center within its octahedron. Bismuth atoms are linked through I3; the Bi-I distances in the resulting I-Bi-I chains being long [3.3503(6) Å and 3.2628(6) Å], with a Bi-I-Bi angle of 148.947(19)°. The iodine atoms axial to the plane of the chain show Bi-I distances of 2.9691(5) Å and 3.1554(5) Å, with axial I-Bi-I bond angles ranging from 169.508(18)° to 177.241(19)°, whilst the equatorial I-Bi-I bond angles ranged from 83.387(6)° to 98.522(17)°. The equatorial Bi-I distances range from 2.9055(6) Å to 3.3504(6) Å. Hydrogen bonds form between all six of the ammonium hydrogens and all but

one of the iodines, with H···I distances of 2.60(3) to 2.91(6) Å, and corresponding N···I separations of 3.525(7) to 3.629(7) Å (Figure S2). The hydrogen bonds link the one-dimensional chains into a three-dimensional array. The resulting hydrogen bond arrangement is shown in Figure S2.

Table 1: Selected parameters from data collection and refinement for PPD bismuth halides.

	(PPD)BiI_5	**(PPD)$[BiBr_4]_2 \cdot 2H_2O$**	**$(PPD)_2BiCl_7 \cdot H_2O$**
CCDC Code	2180531	2180532	2180533
Formula weight	953.64	601.72	695.46
Crystal description	Red chip	Yellow prism	Colourless prism
Crystal size (mm^3)	0.05×0.03×0.02	0.09×0.06×0.03	0.15×0.13×0.03
Crystal system	Monoclinic	Monoclinic	Triclinic
Space group	$P2_1$	$P2_1/c$	$P\bar{1}$
a (Å)	10.0586(4)	7.2340(17)	9.505(2)
b (Å)	8.4358(3)	12.090(3)	10.376(2)
c (Å)	10.8613(5)	12.753(3)	13.322(3)
α (°)			99.260(4)
β (°)	107.582(4)	98.210(6)	110.582(4)
γ (°)			105.1820(10)
Volume	878.55(6) Å^3	1103.9(5) Å^3	1139.6(4) Å^3
Z	2	4	2
ρ(calc, g/cm^3)	3.605	3.620	2.027
μ (mm^{-1})	18.796	30.397	8.566
F(000)	816	1052	664
Reflections collected	11474	13096	4063
Independent reflections (R_{int})	3734 (0.0285)	2018 (0.0770)	4063 (0.046)
Parameters, restraints	145, 10	106, 28	269, 82
Goodness-of-fit on F^2	1.015	0.968	1.180
R_1	0.0235	0.0394	0.0413
R_1 [I>2sigma(I)]	0.0204	0.0320	0.0402
wR_2	0.0363	0.0757	0.1307
wR_2 [I>2sigma(I)]	0.0357	0.0738	0.1300
Absolute structure parameter	-0.026(3)		
Largest diff. peak and hole (e/Å^3)	0.672 and -0.883	1.680 and -1.815	2.968 and -1.945

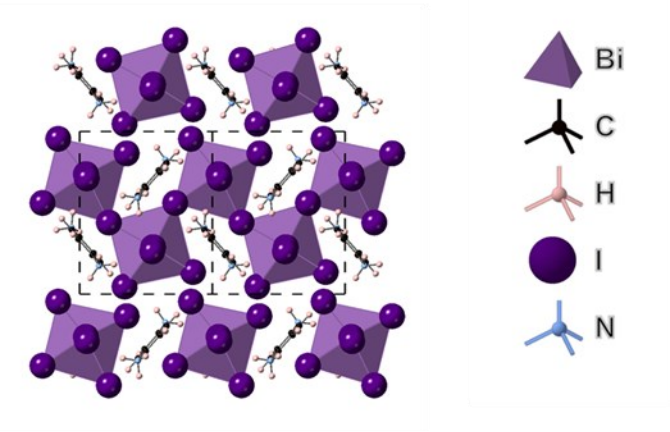

Figure 1: Structure of (PPD)BiI_5 obtained from single crystal XRD showing the view in the *bc* plane, indicating corner-sharing BiI_6 octahedra which run along the *b*-axis.

The PPD bismuth iodide system is particularly interesting as a number of different structures have been reported. A summary of structural data from the Cambridge Structural Database[40] are included in Table S1.[24, 25, 27] Shestimerova *et al.* prepared (PPD)$(BiI_4)_2{\cdot}I_2$, which contains zig-zag, one-dimensional chains of edge sharing BiI_6 octahedra running along the *a*-axis.[27] The shortest inter-chain I-I distance is 3.837(1)Å along the *c*-axis and 3.862(1)Å along the *b*-axis. As suggested in the formula (PPD)$(BiI_4)_2{\cdot}I_2$, the material contains discrete iodine molecules, with an I-I distance of 2.7286(9) Å, which is typical of that found in molecular iodine (2.722(3) Å) at similar temperatures.[27, 41] Hrizi *et al.* have studied α- and β-$(PPD)_2Bi_2I_{10}$ and a corresponding hydrate.[24, 25] These structures both contain isolated dimers of edge sharing bismuth iodide octahedra, forming Bi_2I_{10} units. Our new material, (PPD)BiI_5 is therefore the first PPD bismuth iodide to contain corner-sharing BiI_6 octahedra. The I-Bi-I angles in (PPD)BiI_5 vary further from 90° than other reported PPD bismuth iodides (see Table S1). It is also interesting to note that in (PPD)BiI_5, the Bi-Bi distances of 6.3718(4) Å are much longer than Bi-Bi distances in the other PPD bismuth iodides, which range from 4.5122(14) Å to 4.770(5) Å.[24, 25, 27] Interestingly, the Bi-Bi distance in PPDBiI_5 is comparable to the Pb-Pb distances in $(CH_3NH_3)PbI_3$, which has a Pb-Pb distance of 6.306 Å in the cubic $Pm\bar{3}m$ phase at 350 K.[42]

The preliminary PXRD pattern of the sample of $(PPD)BiI_5$ which the single-crystal studied had come from indicated that three phases were present (Figure S3). Optimization of the synthetic procedure resulted in isolation of the second phase present as a pure phase: the PXRD pattern is shown in Figure 2. The PXRD data can be indexed to a monoclinic cell of a = 11.488(3) Å, b = 12.9039(13) Å, c = 15.026(6) Å, β= 112.520(9)°, space group $P2_1/n$. This is in agreement with the published structural model of β-$(PPD)_2Bi_2I_{10}$. The resulting Pawley fit to the PXRD data is shown in Figure 2. The structure of β-$(PPD)_2Bi_2I_{10}$ is shown in Figure S4 and consists of isolated dimers of edge-sharing BiI_6 octahedra, forming Bi_2I_{10} units and therefore can be described as a zero dimensional perovskite.[24] This is structurally very different to $(PPD)BiI_5$, which consists of chains of corner-sharing octahedra forming one-dimensional chains. Attempts to prepare $(PPD)BiI_5$, in a pure form were unsuccessful, so further studies focused solely on β-$(PPD)_2Bi_2I_{10}$.

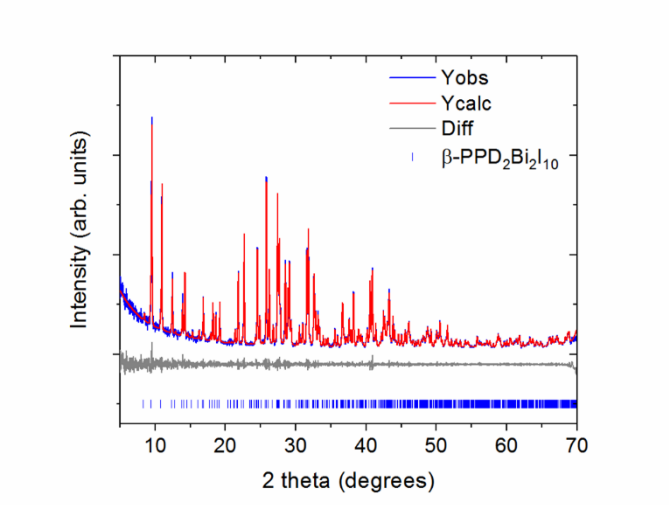

Figure 2: Pawley fit to PXRD data obtained for β-$(PPD)_2Bi_2I_{10}$

It was previously shown that the different compounds β-$(PPD)_2Bi_2I_{10}$ and its hydrate $(PPD)_2Bi_2I_{10}$•$4H_2O$ are structurally very similar, showing a small difference in unit cell parameters, which makes it difficult to distinguish between the two forms using powder X-ray diffraction.[24, 25] In order to investigate the possible incorporation of water into β-$(PPD)_2Bi_2I_{10}$

sample, a combined TGA-DTA experiment was carried out (Figure 3). A mass loss of 0.4% occurred between 50 and 60 °C and is accompanied by an exothermic peak in the DTA. This mass loss is smaller than the 3.6% expected for complete loss of all four water molecules in $(PPD)_2Bi_2I_{10}\cdot 4H_2O$, and is equivalent to the presence of 0.4 H_2O per $(PPD)_2Bi_2I_{10}$ formula unit. This provides preliminary evidence for the accommodation of a variable water content (*i.e.* a region of solid solution) in $(PPD)_2Bi_2I_{10}\cdot xH_2O$, where based on literature and our current work, x can range from 0 to 4.

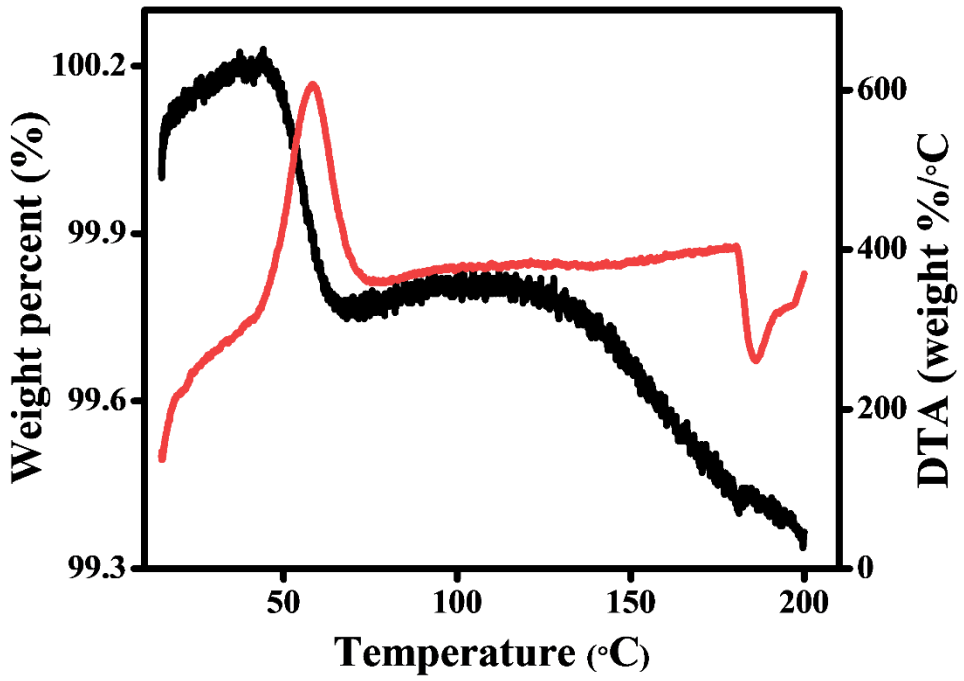

Figure 3: Thermogravimetric analysis (TGA) and differential thermal analysis (DTA) of β-$(PPD)_2Bi_2I_{10}$ carried out under an air atmosphere, black line represents TGA and red line represents the DTA

The structure of $(PPD)[BiBr_4]_2\cdot 2H_2O$ was determined from single crystal XRD data and is shown in Figure 4. It crystallises in the space group $P2_1/c$ and consists of one-dimensional chains of edge sharing $BiBr_6$ octahedra, which run along the a-axis in a zig-zag motif. The PPD cation is positioned in the spaces between chains of $BiBr_6$ octahedra. The asymmetric unit

comprises of one bismuth atom, four crystallographically independent Br atoms, half a PPD cation and a molecule of water. The Bi-Br bond lengths range between 2.6619(11) Å and 3.1251(11) Å (Table 2), with Br-Bi-Br bond angles ranging from 83.86(3)° to 95.82(4)°. Bismuth atoms are linked alternately through Br2 and Br3 atoms; each pair of bringing Br atoms binding asymmetrically, showing one longer and one shorter bond [2.8474(10) and 3.1251(11), and 2.8832(10) and 3.1228(10) for Br2 and Br3, respectively], with Bi-Br-Bi angles of 92.85(3)° and 92.70(3)°, for Br2 and Br3, indicating some distortion of the bismuth octahedra. The inter-chain Br-Br distance is 3.8173(15) Å. Each potential hydrogen bond donor, both ammonium and water, forms a single hydrogen bond, two N-H···Br, one N-H···O and two O-H···Br. These show N-H···Br distances of 2.582(17) and 2.69(5) Å [N···Br separations of 3.518(8) and 3.564(8) Å], an N-H···O distance of 1.73(19) Å [N···O separation of 2.713(10) Å], and O-H···Br distances of 2.49(2) and 2.61(5) Å [O···Br separations of 3.451(8) to 3.508(8) Å]. The hydrogen bonds link the one-dimensional chains into a three-dimensional array (Figure S5).

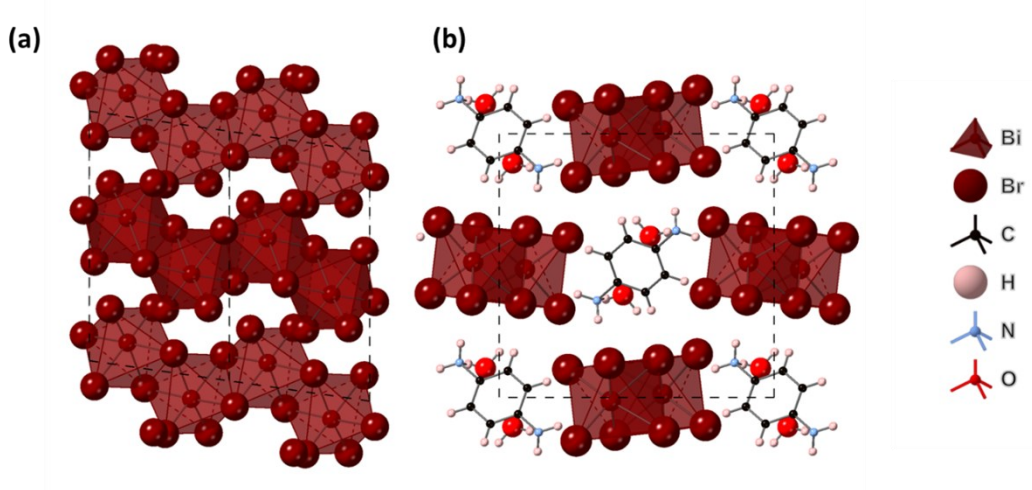

Figure 4: Structure of (PPD)[$BiBr_4$]$_2$·2H_2O obtained from single crystal XRD (a) *ac* plane (showing only chains of $BiBr_6$ octahedra without the PPD cation for clarity) and (b) *bc* plane.

The powder X-ray diffraction pattern of (PPD)[$BiBr_4$]$_2$·2H_2O is shown in Figure S6 and could be indexed to the same monoclinic cell as the single crystal XRD data. The resulting Pawley

fit is shown in Figure S6. A very small percentage of a secondary phase, attributed to the bromide analogue of β-$(PPD)_2Bi_2I_{10}$, was present in the powder X-ray diffraction pattern. This will be discussed in a future publication.

The structure of $(PPD)_2BiCl_7 \cdot H_2O$ was determined from single crystal XRD data and is shown in Figure 5. It crystallizes in the space group $P\bar{1}$ and the bismuth chloride motif consists of contains isolated $BiCl_6$ octahedra. This is in contrast to the other PPD bismuth halides synthesized in this study, which showed either dimers or chains of octahedra. The closest inter-octahedra Cl-Cl distance is 4.836(4) Å. The asymmetric unit comprises one bismuth atom, seven crystallographically independent Cl atoms, (one not coordinated), one whole and two half crystallographically independent PPD cations and a molecule of water. The Bi-Cl bond lengths range from 2.567(3) to 2.941(3) Å (Table 2), with Cl-Bi-Cl bond angles ranging from 84.35(8) to 94.29(9)°. The Bi-Cl distances cluster with three shorter and three longer. Each potential ammonium hydrogen-bond donor, forms at least one hydrogen bond; all bar one to chloride, while the water forms three hydrogen bonds to chlorides. These show N-H···Cl distances ranging from 2.20(2) to 2.84(9) Å [N···Cl separations of 3.133(10) to 3.317(9) Å], an N-H···O distance of 1.84(4) Å [N···O separation of 2.786(16) Å], and O-H···Cl distances of 2.55(8) to 2.81(10) Å [O···Cl separations of 3.278(10) to 3.428(10) Å]. The hydrogen bonds link the $BiCl_6$ octahedra into a three-dimensional array.

Figure 6 shows a comparison of the Bi-X octahedra in the three materials and the corresponding bond lengths are summarized in Table 2.

It is interesting to note that a polymorph of $(PPD)_2BiCl_7 \cdot H_2O$ has been reported previously by Hrizi *et al.* although the synthetic conditions are different to those used here and the resulting structure is different to the $(PPD)_2BiCl_7 \cdot H_2O$ that we report here, with an approximate doubling of the *b*-axis.[26] Attempts to fit our PXRD data with the model/cell

parameters previously reported by Hrizi *et al.*[26] were unsuccessful, using both Rietveld and Pawley refinement. However, our PXRD data could be fitted with the unit cell parameters that we obtained from single crystal X-ray diffraction (see Figure S7), indicating the difference in the unit cell parameters and structures of the two materials. PXRD data were collected after 8 months, to judge the long-term stability of the samples and are shown in Figure S8. The SEM images of the samples synthesized are shown in Figure S9. A detailed description of crystallographic parameters of the *p*-phenylenediammonium bismuth halides (PPD)BiI_5, (PPD)$[BiBr_4]_2 \cdot 2H_2O$ and $(PPD)_2BiCl_7 \cdot H_2O$ are given in Table 2 and Table S2. The FTIR spectra are shown in Figure S10 and Table S3 summarizes the characteristic vibrational frequencies of these materials.

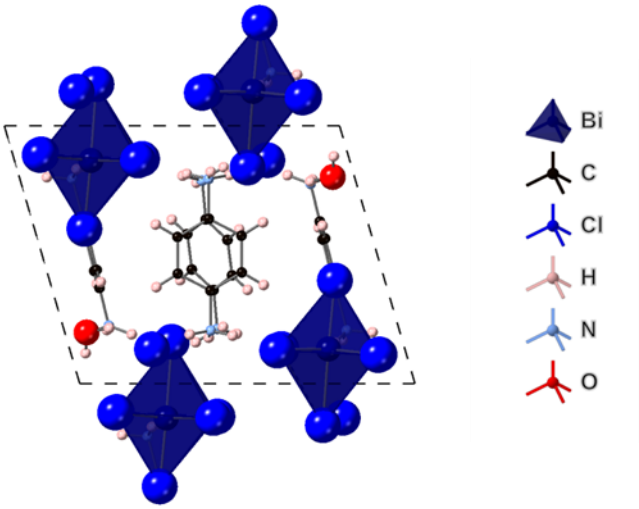

Figure 5: Structure of $(PPD)_2BiCl_7 \cdot H_2O$ when viewed along the *a*-axis.

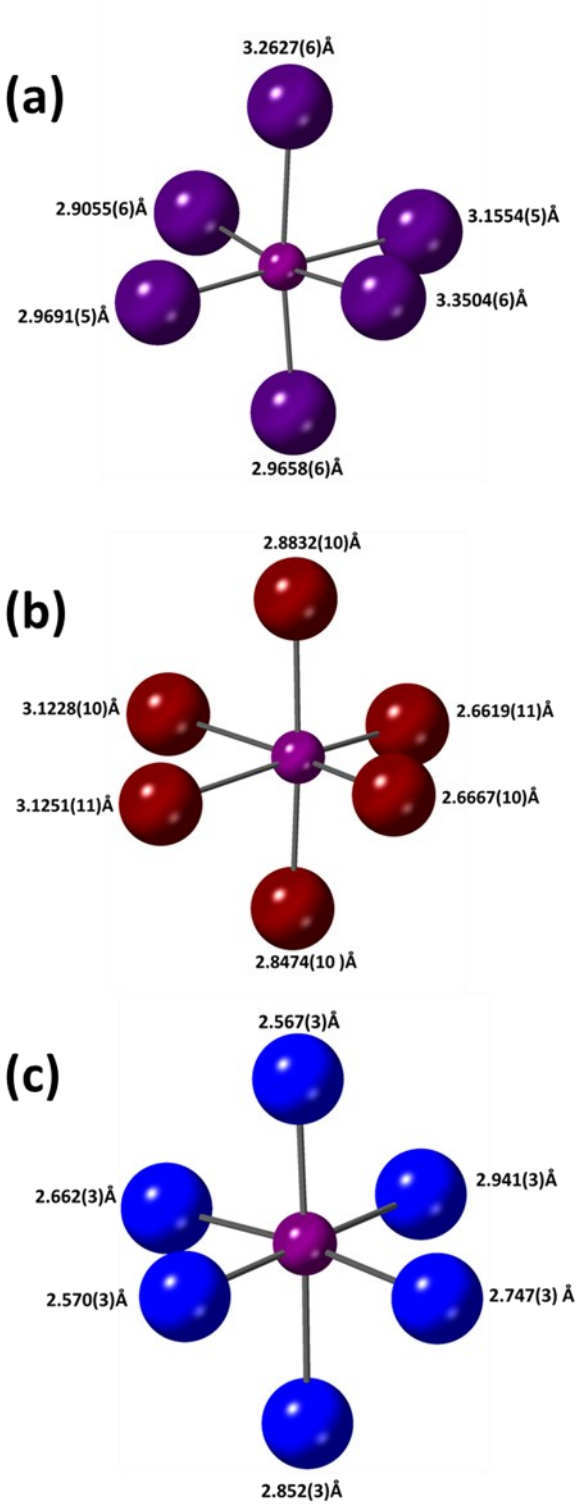

Figure 6: Bond lengths in Bi-X octahedra for (a) BiI_6 (b) $BiBr_6$ and (c) $BiCl_6$ in the structures of (PPD)BiI_5, (PPD)$[BiBr_4]_2 \cdot 2H_2O$ and (PPD)$_2BiCl_7 \cdot H_2O$. Bi is the central atom, I is purple, Br is dark red and Cl is blue.

Table 2: Selected Bi-X (X = I, Br, Cl) bond lengths in $(PPD)BiI_5$, $(PPD)[BiBr_4]_2{\cdot}2H_2O$ and $(PPD)_2BiCl_7{\cdot}H_2O$ and β-$(PPD)_2Bi_2I_{10}$. The bond length distortion, Δd and bond angle variance σ^2 have been calculated using the method described by Robinson *et al.* and these terms are commonly used to quantify polyhedral distortion.[43] Bond length distortion is given by $\Delta d = \frac{1}{6}\sum\left[\frac{d_n - d}{d}\right]^2$ and bond angle variance is given by $\sigma = \sum_{i=1}^{12}\frac{(\theta-90)^2}{11}$.

	$(PPD)BiI_5$	$(PPD)[BiBr_4]_2{\cdot}2H_2O$	$(PPD)_2BiCl_7{\cdot}H_2O$	β-$(PPD)_2Bi_2I_{10}$
	Bi-I (Å)	**Bi-Br (Å)**	**Bi-Cl (Å)**	**Bi-I (Å)**
Bi-X(Å)	2.9055(6)	2.6619(11)	2.567(3)	2.923(3)
Bi-X(Å)	2.9658(6)	2.6667(10)	2.569(3)	2.951(3)
Bi-X(Å)	2.9691(5)	2.8474(10)	2.662(3)	3.064(2)
Bi-X(Å)	3.1554(5)	2.8832(10)	2.747(3)	3.1013(19)
Bi-X(Å)	3.2627(6)	3.1228(10)	2.852(3)	3.246(3)
Bi-X(Å)	3.3504(6)	3.1251(11)	2.941(3)	3.271(3)
Δd ($\times 10^{-4}$)	28.62	42.67	26.19	18.31
σ^2	16.72	12.21	19.52	1.65

3.2 Optoelectronic Properties

The optical behavior of the powdered samples β-$(PPD)_2Bi_2I_{10}$, $(PPD)[BiBr_4]_2{\cdot}2H_2O$ and $(PPD)_2BiCl_7{\cdot}H_2O$ were determined by UV-Visible absorption and photoluminescence (PL) spectroscopies. Figure 7a-c shows the absorption spectra of β-$(PPD)_2Bi_2I_{10}$, $(PPD)[BiBr_4]_2{\cdot}2H_2O$ and $(PPD)_2BiCl_7{\cdot}2H_2O$ with corresponding band gaps, assessed by the Tauc plot[44] (Figure 7d). In compound β-$(PPD)_2Bi_2I_{10}$, a clear band edge from electronic absorption is observed at 1.83 eV (680 nm). In 3D perovskites, the absorption onset in the low energy region is correlated with the largest Bi-I-Bi bond angles, which favoured the formation of a low energy conduction band and leads to a low band gap.[45] Table 3 summarizes the band gaps of other bismuth-containing halides. It can be seen that the band gap of 1.83 eV reported here for β-$(PPD)_2Bi_2I_{10}$ is low and comparable to those reported for other hybrid bismuth halides. This is desirable because it brings it close to the optimum bandgap of 1.5 eV for a single junction solar cell.[46] Therefore, it may be a possible candidate for lead-free light harvesting materials in solar cells. The band gap of $(PPD)[BiBr_4]_2{\cdot}2H_2O$ is 2.64 eV, and was determined from the Tauc plot with the absorption cutoff wavelength set at at 480 nm. Similarly, the data pertaining to $(PPD)_2BiCl_7{\cdot}H_2O$ showed the absorption cutoff at a

wavelength of 395 nm. This compound has a higher octahedral distortion (in terms of bond angle variance, see Table 2) and from the Tauc plot the band gap was determined to be 2.93 eV. A clear red shift was observed from compound $(PPD)_2BiCl_7 \cdot H_2O$ to β-$(PPD)_2Bi_2I_{10}$. The PPD bismuth halides are able to support different connectivities of BiX_6 octahedra, which results in different levels of octahedral distortion for $(PPD)BiI_5$, $(PPD)[BiBr_4]_2 \cdot 2H_2O$ and $(PPD)_2BiCl_7 \cdot H_2O$ and β-$(PPD)_2Bi_2I_{10}$ (Table 2). By changing the halide ions, we are able to produce new materials with different band gaps, which may have applications in a range of optoelectronic devices.[47,48]

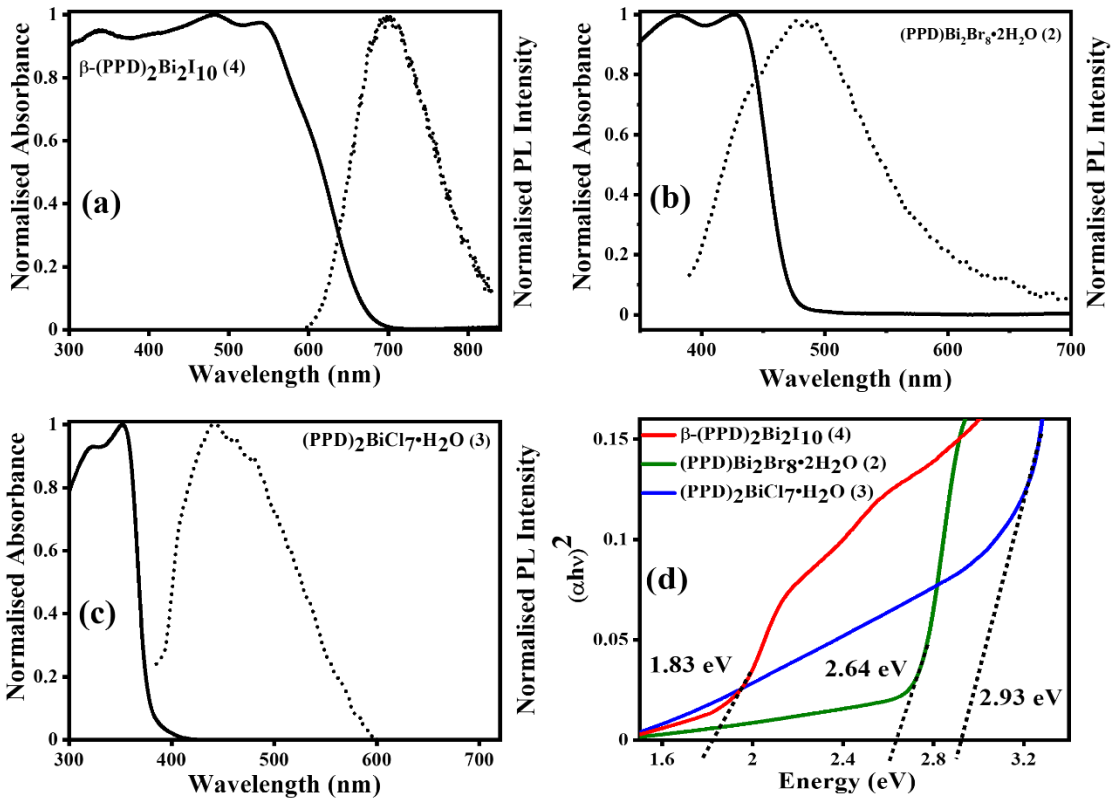

Figure 7: Absorption (solid lines) and photoluminescence (PL) (dotted lines) spectra of (a) β-$(PPD)_2Bi_2I_{10}$, (b) $(PPD)[BiBr_4]_2 \cdot 2H_2O$, (c) $(PPD)_2BiCl_7 \cdot H_2O$, (d) Tauc plot of β-$(PPD)_2Bi_2I_{10}$ (red), $(PPD)[BiBr_4]_2 \cdot 2H_2O$ (olive) and $(PPD)_2BiCl_7 \cdot H_2O$ (blue). The PL spectra were collected following excitation at 430 nm for β-$(PPD)_2Bi_2I_{10}$ and at 350 nm for $(PPD)_2BiCl_7 \cdot H_2O$ and $(PPD)[BiBr_4]_2 \cdot 2H_2O$.

Table 3: Band gaps of some bismuth containing perovskite materials

Compound	Band gap (eV)	Techniques	Reference
$Cs_2AgBiBr_6$	2.02	top-seeded solution growth (TSSG) method.	[49]
$Cs_2AgBiBr_6$	2.19	solid state grinding and solution precipitation	[50]
$Cs_2AgBiCl_6$	2.77	solid state grinding and solution precipitation	[50]
$(CH_3NH_3)_2AgBiBr_6$	2.02	hydrothermal method	[51]
$(CH_3NH_3)_2KBiCl_6$	3.04	hydrothermal method	[52]
$(CH_3NH_3)_2TlBiBr_6$	2.16	hydrothermal method	[20]
$(TMP)[BiI_5]$	2.02	solvothermal method	[53]
$(TMP)[BiBr_5]$	2.67	solvothermal method	[53]
$(TMP)[BiCl_5]$	3.21	solvothermal method	[53]
$(TMP)_{1.5}[Bi_2I_7Cl_2]$	2.10	solvothermal method	[53]
$(C_6H_{13}N)_2BiI_5$	2.02	slow evaporation method	[54]
$(CH_3NH_3)_3Bi_2I_9$	2.06	solution grown powder method	[55]
$(CH_3NH_3)_3Bi_2I_9$	2.19	thin film in mixed solvents	[14]
$(CH_3NH_3)_3Bi_2I_9$	2.10	thin film formation in mixed solvents	[56]
$Cs_3Bi_2I_9$	2.20	thin film formation in mixed solvents	[56]
$AgBi_2I_7$	1.87	solution processed thin film method	[57]
$[H_3N(CH_2)_6NH_3]BiI_5$	1.89	slow cooling solution method	[58]
Cs_2NaBiI_6	2.43	first principle study	[59]
$(CH_3NH_3)_3Bi_2Br_9$	2.5	collaborative solvent ligand-assisted re-precipitation method	[60]
$(C_3H_5N_2S)BiI_4$	1.78	solution growth using solvent layering approach	[61]
$KBiI_4 \cdot H_2O$	1.76	slow evaporation method	[62]
1,1-(1,n-Alkanediyl)bis(4-methylpyridinium)BiI_5 /$H_3C(C_5H_4N)(CH_2)_5(C_5H_4N)CH_3$	1.73	slow evaporation from solution.	[63]
$(C_{17}H_{18}N_4)BiI_5$	1.59	solution growth	[64]
$(AmV)BiI_5$ (AmV^{2+} = 4,4′-amino-bipyridinium)	1.54	slow evaporation	[65]
$[(Me_2DABCO)2(Bi_2I_{10})_2]$ [DABCO = 1,4-diazabicyclo[2.2.2]octane]	1.44	solvothermal with slow cooling	[66]

The room temperature steady state photoluminescence (PL) spectra of thin films of β-$(PPD)_2Bi_2I_{10}$, $(PPD)[BiBr_4]_2{\cdot}2H_2O$ and $(PPD)_2BiCl_7{\cdot}2H_2O$ are shown in Figure 7 (a-c). The PL of β-$(PPD)_2Bi_2I_{10}$ shows a broad emission peak at 703 nm with a full width half maximum (FWHM) of 119 nm and a separation between the longest wavelength absorption peak and the emission maximum of 164 nm. Compound $(PPD)[BiBr_4]_2{\cdot}2H_2O$ shows a broad PL emission around 477 nm with FWHM of 146 nm and a shift of 51 nm between absorption and emission. The PL of $(PPD)_2BiCl_7{\cdot}H_2O$ has a peak around 443 nm with a FWHM of 130 nm and has a peak around 443 nm. The shift between absorption and emission maxima is 91 nm. Table 4 represents the characteristic parameters of β-$(PPD)_2Bi_2I_{10}$, $(PPD)[BiBr_4]_2{\cdot}2H_2O$ and $(PPD)_2BiCl_7{\cdot}2H_2O$ deduced from UV-Vis and SSPL. According to Karunadasa *et al*. the broad emission is attributed to emission from defect sites which lead to the self-trapping of excitons and the distortion of the crystal structure.[67] This distortion in the crystal structure has a strong correlation with the broadband light emission.[68, 69] There are three aspects of the crystal structure which have been attributed to the broad emission spectra. First, the chloride ions in these materials cause more octahedral distortion due to their small size compared to the other halide anions. Second, the rigid PPD cation also enhances octahedral distortion and contributes to the width of the PL peaks. Third, more hydrogen bonds form between the octahedra and diammonium cations than for monoammonium cations in perovskite structures enables the stronger interaction, which is also responsible for self-trapping of excitons for broad emission in perovskite materials.[70]

A long exciton lifetime is desirable for efficient charge transfer and extraction. It is dependent on a number of parameters, but in general single crystals or films with a large grain size exhibit the highest charge carrier lifetimes. Materials which have optimum band gaps and long charge carrier lifetimes can result in photovoltaic devices with higher efficiency. However, the presence of defects or impurities quenches the light emission and is a major non-radiative loss

pathway in perovskites. These defects are mostly due to surface halide vacancies.[71] It has been shown that oxygen passivation can suppress these trap states efficiently.[72, 73] We have investigated oxygen passivation by spin-coating the films in the presence and absence of oxygen, i.e. outside and inside a nitrogen-filled glovebox. The time-resolved PL decays of spin-coated films of β-$(PPD)_2Bi_2I_{10}$ with and without oxygen passivation are shown in Figure 8(a). We found that the charge carrier lifetime of the film spin-coated in air is significantly enhanced compared to the film spin-coated inside the glovebox. Oxygen molecules are believed to bind strongly to surface halide vacancies and form superoxide in the presence of photo-excited electrons, which then leads to efficient passivation of these vacancy sites.[74]

Table 4 Characteristics parameters of β-$(PPD)_2Bi_2I_{10}$ (4), $(PPD)[BiBr_4]_2{\cdot}2H_2O$ (2) and $(PPD)_2BiCl_7{\cdot}2H_2O$ (3) deduced from UV-Vis and SSPL.

Compound	**Absorption Cutoff (nm)**	**Absorption Peak (nm)**	**Band Gap (eV)**	**PL Peak (nm)**	**FWHM (nm)**	**Stokes Shift (nm)**	**Stokes Shift (eV)**
β-$(PPD)_2Bi_2I_{10}$ (4)	680	539	1.83	703	119	164	0.54
$(PPD)[BiBr_4]_2{\cdot}2H_2O$ (2)	480	426	2.64	477	146	51	0.31
$(PPD)_2BiCl_7{\cdot}H_2O$ (3)	395	352	2.93	443	130	91	0.72

PL decays of passivated films of the other materials are shown in Figure 8b. For comparison, the PL decay of passivated film of β-$(PPD)_2Bi_2I_{10}$ is also plotted in Figure 8b. The PL of compounds $(PPD)[BiBr_4]_2{\cdot}2H_2O$ and $(PPD)_2BiCl_7{\cdot}H_2O$ decayed completely within 200 ns, whereas β-$(PPD)_2Bi_2I_{10}$ showed a much slower PL decay after fast initial decay. In order to get information about different processes, the PL decays of compounds $(PPD)[BiBr_4]_2{\cdot}2H_2O$ and

$(PPD)_2BiCl_7 \cdot H_2O$ were fitted with equation (1) and the fitting parameters are given in Table 5.

$$R(t) = A_1 e^{(-t/\tau_1)} + A_2 e^{(-t/\tau_2)} + A_3 e^{(-t/\tau_3)} \qquad (1)$$

where A_1, A_2 and A_3 are pre-exponential factors. The relative fluorescence intensity or yield (%) of each component calculated using equation (2)[73] and given in Table 5.

$$\varphi_n = \frac{A_n \tau_n}{A_1\tau_1 + A_2\tau_2 + A_3\tau_3} \times 100 \qquad (2)$$

The long lifetime of β-$(PPD)_2Bi_2I_{10}$ was further investigated by measuring the PL decay up to 3 μs (Figure 8c). Fitting of the PL data with three exponentials (Equation 1) yields a fast component with lifetime of ~8 ns (11 %), an intermediate component with lifetime of τ_2 = ~124 ns (10 %) and a very long component with lifetime of τ_3 =1260 ns (79 %). The fast (τ_1) and intermediate (τ_2) components may result from traps and/or surface states, whereas the slow decay component τ_3 is related to the natural recombination of carriers in β-$PPD_2Bi_2I_{10}$.[75] The long recombination lifetime (>1μs) is comparable to that of $(CH_3NH_3)PbI_3$ and is significantly higher than that of other optimized layered perovskites.[76] The long recombination lifetime is promising for photovoltaic applications because it provides enough time for the excitons to be dissociated into free charges at the interface.[77]

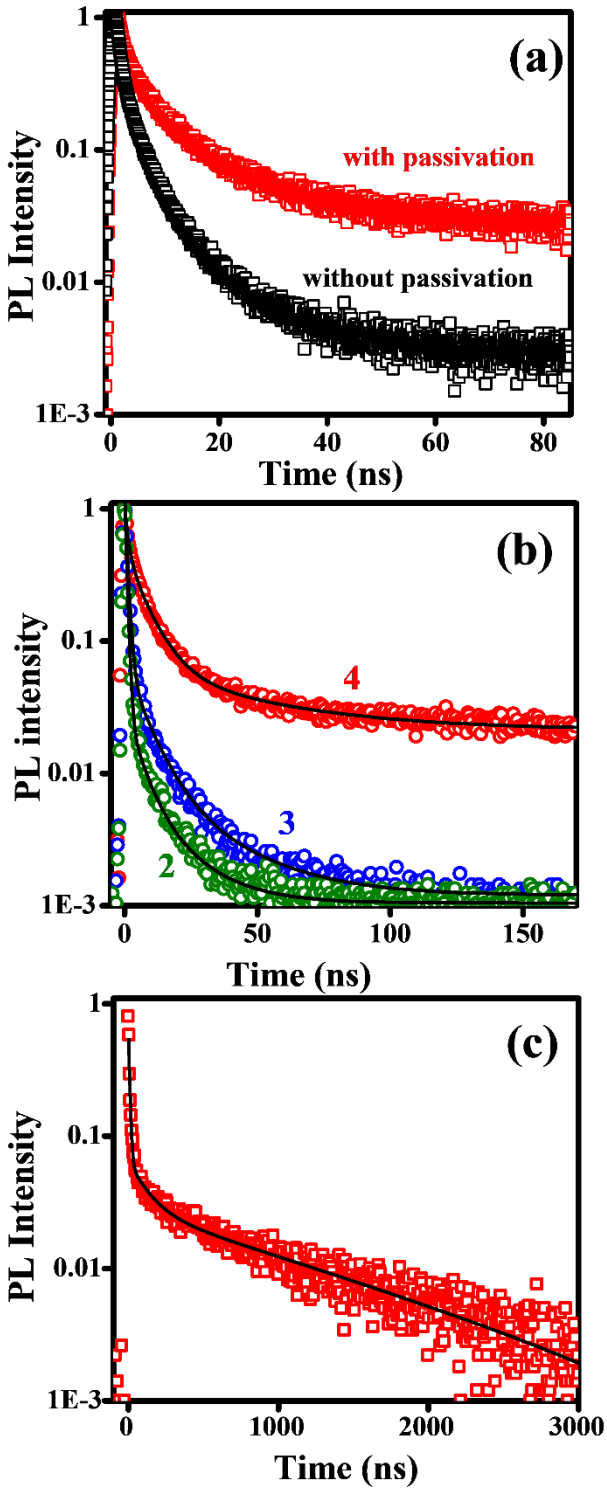

Figure 8: Time-resolved PL decays of bismuth containing perovskite thin films, following excitation at 379 nm by a picosecond pulsed laser. (a) Effect of oxygen passivation on β-$(PPD)_2Bi_2I_{10}$. The red curve ("with passivation") is a decay of a film sample spin-coated in air. The black curve ("without passivation") is a decay of a film a sample spin-coated in a nitrogen glove box. (b) PL decays of oxygen-passivated films of $(PPD)_2BiCl_7{\cdot}H_2O$ (3,blue), $(PPD)[BiBr_4]_2{\cdot}2H_2O$ (2, olive) and β-$(PPD)_2Bi_2I_{10}$ (4, red) Black lines are three-exponential fit to the experimental data using equation 1. (c) PL decay of β-$(PPD)_2Bi_2I_{10}$ measured up to 3 μs. Black line is three-exponential fit.

Table 5: Tri-exponential decay fitting parameters of β-$(PPD)_2Bi_2I_{10}$, $(PPD)[BiBr_4]_2{\cdot}2H_2O$ and $(PPD)_2BiCl_7{\cdot}H_2O$.

Compound	τ_1	τ_2	τ_3
β-$(PPD)_2Bi_2I_{10}$	8.2 ns (11.3%)	123.6 ns (10.0%)	1260.4 ns (78.7%)
$(PPD)[BiBr_4]_2{\cdot}2H_2O$	0.7 ns (65.7%)	4.8 ns (21.2%)	130.3 ns (13.1%)
$(PPD)_2BiCl_7{\bullet}H_2O$	0.9 ns (57.1%)	8.8 ns (32.5%)	46.5 ns (10.4%)

To facilitate an approximate comparison with prior work we calculated the average PL lifetime using the intensity weighted average of the fitted exponentials by using equation (3) and the calculated average lifetimes are given in Table 5.

$$\tau_{avg} = \frac{A_1\tau_1^2+A_2\tau_2^2+A_3\tau_3^2}{A_1\tau_1+A_2\tau_2+A_3\tau_3} \quad (3)$$

Table 6: The PL lifetime (τ_{verage}) of some perovskite halides (PEA = phenylethylammonium, BPMA = 4-biphenylmethylammonium, BA = butylammonium, DMEN = (2-dimethylamino)ethylammonium, PPD = *p*-phenyldiammonium) .

Compound	$\tau_{average}$	Techniques	Reference
$(CH_3NH_3)PbI_3$	1500 ns	TR microwave conductance	[78]
$(CH_3NH_3)PbI_3$	6.6 ns	TRPL-FTO/TiO_2r/perovskite	[79]
$(CH_3NH_3)PbI_3$	390 ns	transient photovoltage method	[80]
$(CH_3NH_3)Pb(I_{0.71}Br_{0.29})_3$	560 ns	transient photovoltage method	[80]
$(CH_3NH_3)Pb(I_{0.46}Br_{0.54})_3$	1070 ns	transient photovoltage method	[80]
$(CH_3NH_3)PbI_3$	208 ns	TRPL-vapor-equilibrated method	[81]
$(CH_3NH_3)PbCl_xI_{3-x}$	113.9 ns	TRPL-vapor-equilibrated method	[81]
$CsPbBr_3$	5.6 ns	TRPL- thiocyanate treatment	[82]
$CsPbBr_3$	16.8 ns	TRPL-SiO_2 core shell	[83]
$CsPbBr_3$	3.9 ns	TRPL-pristine	[84]
$CsPbBr_3$	6.5 ns	TRPL-in situ passivation	[84]
$(CH_5N_2)PbBr_3$	180.3 ns	TRPL-Rubidium doping	[85]
$(CH_3NH_3)PbBr_3$	10.1 ns	TRPL-with benzoquinone	[86]
$(CH_3NH_3)PbBr_3$	7.07 ns	TRPL	[87]
Cs_4PbBr_6	1.9 ps	femtosecond TA	[88]
$(PEA)_2PbI_4[(CH_3NH_3)PbI_3]_{n-1}$ (1,2,3)	~150 ps	TRPL	[89]
$Cs_2InCl_5{\bullet}H_2O$	4.2 μs	TRPL	[90]
$(BPMA)_2PbBr_4$	4.73 ms	Transient fluorescence	[91]
$(C_4N_2H_{14})PbBr_4$	201 ns	pressure-induced PL	[92]
$(C_4H_{14}N_2)_2In_2Br_{10}$	3.2 μs	TRPL	[93]
$(BA)_{2(}CH_3NH_3)_4Pb5I_{16-10x}Br_{10x}$	3.47 ns	TRPL	[94]
$(p\text{-}FC_6H_4C_2H_4NH_3)_2[PbI_4]$	63 ns	TRPL	[95]
$(DMEN)PbBr_4$	0.75 μs	TRPL	[96]
β-$(PPD)_2Bi_2I_{10}$	1245 ns	TRPL	This work
$(PPD)[BiBr_4]_2{\cdot}2H_2O$	120 ns	TRPL	This work
$(PPD)_2BiCl_7{\cdot}H_2O$	31 ns	TRPL	This work

We note that measured charge carrier lifetimes are affected by factors such as the size of crystallites, uniformity of the film and rate of surface recombination, hence Table 6 shows a range of lifetimes for materials with the same reported chemical composition. Nevertheless, the charge carrier lifetime reported in this work for β-$(PPD)_2Bi_2I_{10}$ is one of the longest reported to date.[77, 79, 80]

4. Conclusions

We have successfully synthesized PPD bismuth halides using a slow cooling solution method. Here, three new perovskite materials were prepared, $(PPD)BiI_5$, $(PPD)[BiBr_4]_2{\cdot}2H_2O$ and $(PPD)_2BiCl_7{\cdot}H_2O$. They differed in their connectivity of bismuth halide octahedra and also in the ratio of organic: inorganic cations. We also prepared β-$(PPD)_2Bi_2I_{10}$. The long-term ambient stability and long charge carrier lifetimes suggests that these materials have potential applications in photovoltaic devices. Specifically, β-$(PPD)_2Bi_2I_{10}$ has a small band gap (1.83 eV) and also exhibited long charge carrier lifetime of ~1.2 μs, which is comparable to $(CH_3NH_3)PbI_3$ and suggests that has potential for lead-free hybrid perovskite photovoltaic devices.

Acknowledgements:

ZS acknowledges Higher Education Commission (HEC) of Pakistan for indigenous PhD Fellowship Phase-II, Batch II, 2013, PIN 213-66018-2PS2-127 and International Research Support Initiative Programme (IRSIP). She also acknowledges a British council of Pakistan for Pakistan Scottish PhD Research Travel Grants for Women 2017-18. JLP thanks the University of St Andrews for funding and the Carnegie Trust for a Research Incentive Grant (RIG008653). We thank EPSRC for funding (EP/P007821/1).

References

1. K. G. Reddy, T. G. Deepak, G. S. Anjusree, S. Thomas, S. Vadukumpully, K. R. V. Subramanian, S. V. Nair and A. S. Nair, *Phys. Chem. Chem. Phys.*, 2014, **16**, 6838-6858.
2. A. Hagfeldt, G. Boschloo, L. C. Sun, L. Kloo and H. Pettersson, *Chem. Rev.*, 2010, **110**, 6595-6663.
3. F. Bella, *Electrochim. Acta*, 2015, **175**, 151-161.
4. P. Nagarjuna, K. Narayanaswamy, T. Swetha, G. H. Rao, S. P. Singh and G. D. Sharma, *Electrochim. Acta*, 2015, **151**, 21-26.
5. O. Y. Gong, Y. Kim, D. H. Kim, G. S. Han, S. Jeong and H. S. Jung, *ACS Energy Lett.*, 2020, **5**, 1032-1034.
6. J. L. Yang, Y. Yu, L. Y. Zeng, Y. T. Li, Y. Q. Pang, F. Q. Huang and B. L. Lin, *J. Nanomater.*, 2017, **2017**.
7. P. P. Boix, S. Agarwala, T. M. Koh, N. Mathews and S. G. Mhaisalkar, *J. Phys. Chem. Lett.*, 2015, **6**, 898-907.
8. L. B. Qiu, L. K. Ono and Y. B. Qi, *Mater. Today Energy*, 2018, **7**, 169-189.
9. T. Leijtens, R. Prasanna, A. Gold-Parker, M. F. Toney and M. D. McGehee, *ACS Energy Lett.*, 2017, **2**, 2159-2165.
10. I. Kopacic, B. Friesenbichler, S. F. Hoefler, B. Kunert, H. Plank, T. Rath and G. Trimmel, *ACS Appl. Energy Mater.*, 2018, **1**, 343-347.
11. H. C. Sansom, G. F. S. Whitehead, M. S. Dyer, M. Zanella, T. D. Manning, M. J. Pitcher, T. J. Whittles, V. R. Dhanak, J. Alaria, J. B. Claridge and M. J. Rosseinsky, *Chem. Mater.*, 2017, **29**, 1538-1549.
12. Q. Zhang, F. Hao, J. B. Li, Y. Y. Zhou, Y. X. Wei and H. Lin, *Sci. Technol. Adv. Mat.*, 2018, **19**, 425-442.
13. S. Oz, J. C. Hebig, E. W. Jung, T. Singh, A. Lepcha, S. Olthof, J. Flohre, Y. J. Gao, R. German, P. H. M. van Loosdrecht, K. Meerholz, T. Kirchartz and S. Mathur, *Sol. Energy Mat. and Sol. C.*, 2016, **158**, 195-201.
14. C. S. Ni, G. Hedley, J. Payne, V. Svrcek, C. McDonald, L. K. Jagadamma, P. Edwards, R. Martin, G. Jain, D. Carolan, D. Mariotti, P. Maguire, I. Samuel and J. Irvine, *Nat. Commun.*, 2017, **8**.
15. W. X. Chai, L. M. Wu, J. Q. Li and L. Chen, *Inorg. Chem.*, 2007, **46**, 1042-1044.
16. X. W. Tong, W. Y. Kong, Y. Y. Wang, J. M. Zhu, L. B. Luo and Z. H. Wang, *ACS Appl. Mater. Inter.*, 2017, **9**, 18977-18985.
17 A. J. Lehner, D. H. Fabini, H. A. Evans, C-A Hébert, S. R. Smock, J. Hu, H. Wang, J. W. Zwanziger, M. L. Chabinyc, and R. Seshadri, *Chem. Mater.*, 2015, **27**, 7137–7148
18. J-J. Wu, Y. Guo, W-D. Yao, W-L. Liu and S-P. Guo, *Dalton Trans.*, 2022,**51**, 4878-4883
19. X. Li, B. Traoré, M. Kepenekian, L. Li, C. C. Stoumpos, P. Guo, J. Even, C. Katan, and M. G. Kanatzidis, Chem. Mater. 2021, 33, 6206−6216
20. Z. Y. Deng, F. X. Wei, S. J. Sun, G. Kieslich, A. K. Cheetham and P. D. Bristowe, *J. Mater. Chem. A*, 2016, **4**, 12025-12029.
21. H. Dammak, A. Yangui, S. Triki, Y. Abid and H. Feki, *J. Lumin.*, 2015, **161**, 214-220.
22. C. C. Stoumpos, D. H. Cao, D. J. Clark, J. Young, J. M. Rondinelli, J. I. Jang, J. T. Hupp and M. G. Kanatzidis, *Chem. Mater.*, 2016, **28**, 2852-2867.
23. S. D. Stranks and H. J. Snaith, *Nat. Nanotechnol.*, 2015, **10**, 391-402.
24. C. Hrizi, A. Trigui, Y. Abid, N. Chniba-Boudjada, P. Bordet and S. Chaabouni, *J. Solid State Chem.*, 2011, **184**, 3336-3344.
25. C. Hrizi, A. Samet, Y. Abid, S. Chaabouni, M. Fliyou and A. Koumina, *J. Mol. Struct.*, 2011, **992**, 96-101.
26. C. Hrizi, C. Chaker and S. Chaabouni, *Ionics*, 2011, **17**, 545-553.
27. T. A. Shestimerova, N. A. Golubev, N. A. Yelavik, M. A. Bykov, A. V. Grigorieva, Z. Wei, E. V. Dikarev and A. V. Shevelkov, *Cryst. Growth Des.*, 2018, **18**, 2572-2578.

28. L. Dobrzycki and K. Wozniak, *CrystEngComm*, 2008, **10**, 577-589.
29. I. C. Smith, E. T. Hoke, D. Solis-Ibarra, M. D. McGehee and H. I. Karunadasa, *Angew. Chem. Int. Ed.*, 2014, **53**, 11232-11235.
30. Z. K. Tan, R. S. Moghaddam, M. L. Lai, P. Docampo, R. Higler, F. Deschler, M. Price, A. Sadhanala, L. M. Pazos, D. Credgington, F. Hanusch, T. Bein, H. J. Snaith and R. H. Friend, *Nat. Nanotechnol.*, 2014, **9**, 687-692.
31. W. Q. Liao, Y. Zhang, C. L. Hu, J. G. Mao, H. Y. Ye, P. F. Li, S. P. D. Huang and R. G. Xiong, *Nat. Commun.*, 2015, **6**.
32. B. R. Sutherland and E. H. Sargent, *Nat. Photonics*, 2016, **10**, 295-302.
33. X. T. Li, J. Hoffman, W. J. Ke, M. Chen, H. Tsai, W. Y. Nie, A. D. Mohite, M. Kepenekian, C. Katan, J. Even, M. R. Wasielewski, C. C. Stoumpos and M. G. Kanatzidis, *J. Am. Chem. Soc.*, 2018, **140**, 12226-12238.
34. *CrystalClear-SM Expert v2.1.* Rigaku Americas*, The Woodlands, Texas, USA, and* Rigaku Corporation*, Tokyo, Japan, 2015.*
35. *CrysAlisPro v1.171.38.46*. Rigaku Oxford Diffraction, Rigaku Corporation, *Oxford, U.K.*, 2015.
36. G. M. Sheldrick, *Acta Crystallogr., Sect. A: Found. Adv*., 2015, ***71***, 3-8.
37. G. M. Sheldrick, *Acta Crystallogr., Sect. C: Struct. Chem*., 2015, **71**, 3-8.
38. L. J. Farrugia, *J. Appl. Crystallogr.*, 2012, **45**, 849-854.
39. Y. Y. Li, C. K. Lin, G. L. Zheng, Z. Y. Cheng, H. You, W. D. Wang and J. Lin, *Chem. Mater.*, 2006, **18**, 3463-3469.
40. C. R. Groom, I. J. Bruno, M. P. Lightfoot and S. C. Ward, *Acta Crystallogr. B*, 2016, **72**, 171-179.
41. R. M. Ibberson, O. Moze and C. Petrillo, *Mol. Phys.*, 1992, **76**, 395-403.
42. P. S. Whitfield, N. Herron, W. E. Guise, K. Page, Y. Q. Cheng, I. Milas and M. K. Crawford, *Sci. Rep.*, 2016, **6**, 35685.
43. K. Robinson, G. V. Gibbs and P. H. Ribbe, *Science*, 1971, **172**, 567-570.
44. X. Chen, Y. Myung, A. Thind, Z. N. Gao, B. Yin, M. K. Shen, S. B. Cho, P. F. Cheng, B. Sadtler, R. Mishra and P. Banerjee, *J. Mater. Chem. A*, 2017, **5**, 24728-24739.
45. M. R. Filip, G. E. Eperon, H. J. Snaith & F. Giustino, *Nature Commun.*, 2014, 5, 5757
46. W. Shockley and H. J. Queisser, *J. Appl. Phys.*, 1961, **32**, 510-&.
47. J. K. Pious, A. Katre, C. Muthu, S. Chakraborty, S. Krishna and V. C. Nair, *Chem. Mater.*, 2019, **31**, 1941-1945.
48. Y. Bekenstein, J. C. Dahl, J. M. Huang, W. T. Osowiecki, J. K. Swabeck, E. M. Chan, P. D. Yang and A. P. Alivisatos, *Nano Lett.*, 2018, **18**, 3502-3508.
49. D. Bartesaghi, A. H. Slavney, M. C. Gelvez-Rueda, B. A. Connor, F. C. Grozema, H. I. Karunadasa and T. J. Savenije, *J. Phys. Chem. C*, 2018, **122**, 4809-4816.
50. E. T. McClure, M. R. Ball, W. Windl and P. M. Woodward, *Chem. Mater.*, 2016, **28**, 1348-1354.
51. F. X. Wei, Z. Y. Deng, S. J. Sun, F. H. Zhang, D. M. Evans, G. Kieslich, S. Tominaka, M. A. Carpenter, J. Zhang, P. D. Bristowe and A. K. Cheetham, *Chem. Mater.*, 2017, **29**, 1089-1094.
52. F. X. Wei, Z. Y. Deng, S. J. Sun, F. Xie, G. Kieslich, D. M. Evans, M. A. Carpenter, P. D. Bristowe and A. K. Cheetham, *Mater. Horiz.*, 2016, **3**, 328-332.
53. M. Q. Li, Y. Q. Hu, L. Y. Bi, H. L. Zhang, Y. Y. Wang and Y. Z. Zheng, *Chem. Mater.*, 2017, **29**, 5463-5467.
54. W. C. Zhang, K. W. Tao, C. M. Ji, Z. H. Sun, S. G. Han, J. Zhang, Z. Y. Wu and J. H. Luo, *Inorg. Chem.*, 2018, **57**, 4239-4243.
55. M. Abulikemu, S. Ould-Chikh, X. H. Miao, E. Alarousu, B. Murali, G. O. N. Ndjawa, J. Barbe, A. El Labban, A. Amassiana and S. Del Gobbo, *J. Mater. Chem. A*, 2016, **4**, 12504-12515.
56. B. W. Park, B. Philippe, X. L. Zhang, H. Rensmo, G. Boschloo and E. M. J. Johansson, *Adv. Mater.*, 2015, **27**, 6806-6813.
57. Y. Kim, Z. Y. Yang, A. Jain, O. Voznyy, G. H. Kim, M. Liu, L. N. Quan, F. P. G. de Arquer, R. Comin, J. Z. Fan and E. H. Sargent, *Angew. Chem. Int. Edit.*, 2016, **55**, 9586-9590.

58. H. Y. Zhang, Z. H. Wei, P. F. Li, Y. Y. Tang, W. Q. Liao, H. Y. Ye, H. Cai and R. G. Xiong, *Angew. Chem. Int. Edit.*, 2018, **57**, 526-530.
59. S. Zhao, K. Yamamoto, S. S. Iikubo, S. Hayase and T. L. Ma, *J. Phys. Chem. Solids*, 2018, **117**, 117-121.
60. M. Y. Leng, Z. W. Chen, Y. Yang, Z. Li, K. Zeng, K. H. Li, G. D. Niu, Y. S. He, Q. C. Zhou and J. Tang, *Angew. Chem. Int. Edit.*, 2016, **55**, 15012-15016.
61 T. Li, Q. Wang, G. S. Nichol, C. A. Morrison, H. Han, Y. Hu and N. Robertson, *Dalton Trans.*, 2018, **47**, 7050-7058
62 N A. Yelovik, A. V. Mironov, M. A. Bykov, A. N. Kuznetsov, A. V. Grigorieva, Z. Wei, E. V. Dikarev, and A. V. Shevelkov, *Inorg. Chem.*, 2016, **55**, 4132–4140
63 V. Yu. Kotov, A. B. Ilyukhin, A. A. Korlyukov, A. F. Smol'yakovcd and S. A. Kozyukhin, *New J. Chem.,* 2018, 42, 6354-6363
64 V. Y., Kotov, A. B.Ilyukhin, A. A.Sadovnikov, K. P. Birin, N. P.Simonenko, H. T. Nguyen, A. E.Baranchikov, S. A.Kozyukhin, *Mendeleev Commun.*, 2017, **27**, 271–273
65 A. Skorokhod, N. Mercier*, M. Allain, M. Manceau, C. Katan, and M. Kepenekian., *Inorg. Chem.,* 2021, **60**, 22, 17123–17131
66 Z-P Zhang, Q-Y Feng, Y-L Wei, Z-Y Gao, Z-W Wang and Y-M Wang, *J. Clust. Sci.*, 2018, **29**, 725–735
67. M. D. Smith, A. Jaffe, E. R. Dohner, A. M. Lindenberg and H. I. Karunadasa, *Chem. Sci.*, 2017, **8**, 4497-4504.
68. O. Nazarenko, M. R. Kotyrba, S. Yakunin, M. Aebli, G. Raino, B. M. Benin, M. Worle and M. V. Kovalenko, *J. Am. Chem. Soc.*, 2018, **140**, 3850-3853.
69. M. D. Smith and H. I. Karunadasa, *Acc. Chem. Res.*, 2018, **51**, 619-627.
70. S. Ahmad, P. Fu, S. W. Yu, Q. Yang, X. Liu, X. C. Wang, X. L. Wang, X. Guo and C. Li, *Joule*, 2019, **3**, 794-806.
71. S. D. Stranks, R. L. Z. Hoye, D. W. Di, R. H. Friend and F. Deschler, *Adv. Mater.*, 2019, **31**.
72. N. Aristidou, C. Eames, I. Sanchez-Molina, X. N. Bu, J. Kosco, M. S. Islam and S. A. Haque, *Nat. Commun.*, 2017, **8**.
73. R. Brenes, C. Eames, V. Bulovic, M. S. Islam and S. D. Stranks, *Adv. Mater.*, 2018, **30**.
74. T. T. Xuan, S. Q. Lou, J. J. Huang, L. Y. Cao, X. F. Yang, H. L. Li and J. Wang, *Nanoscale*, 2018, **10**, 9840-9844.
75. H. Y. Hsu, L. Ji, M. S. Du, J. Zhao, E. T. Yu and A. J. Bard, *J. Phys. Chem. C*, 2016, **120**, 19890-19895.
76. L. F. Chao, T. T. Niu, Y. D. Xia, X. Q. Ran, Y. H. Chen and W. Huang, *J. Phys. Chem. Lett.*, 2019, **10**, 1173-1179.
77. A. H. Slavney, T. Hu, A. M. Lindenberg and H. I. Karunadasa, *J. Am. Chem. Soc.*, 2016, **138**, 2138-2141.
78. Y. Bi, E. M. Hutter, Y. J. Fang, Q. F. Dong, J. S. Huang and T. J. Savenije, *J. Phys. Chem. Lett.*, 2016, **7**, 923-928.
79. A. B. Huang, J. T. Zhu, J. Y. Zheng, Y. Yu, Y. Liu, S. W. Yang, S. H. Bao, L. Lei and P. Jin, *Nanotechnology*, 2017, **28**.
80. D. Kiermasch, P. Rieder, K. Tvingstedt, A. Baumann and V. Dyakonov, *Sci. Rep.*, 2016, **6,** 39333.
81. B. S. Tosun and H. W. Hillhouse, *J. Phys. Chem. Lett.*, 2015, **6**, 2503-2508.
82. B. A. Koscher, J. K. Swabeck, N. D. Bronstein and A. P. Alivisatos, *J. Am. Chem. Soc.*, 2017, **139**, 6566-6569.
83. Q. X. Zhong, M. H. Cao, H. C. Hu, D. Yang, M. Chen, P. L. Li, L. Z. Wu and Q. Zhang, *ACS Nano*, 2018, **12**, 8579-8587.
84. Y. Wu, C. T. Wei, X. M. Li, Y. L. Li, S. C. Qiu, W. Shen, B. Cai, Z. G. Sun, D. D. Yang, Z. T. Deng and H. B. Zeng, *ACS Energy Lett.*, 2018, **3**, 2030-2037.
85. Y. F. Shi, J. Xi, T. Lei, F. Yuan, J. F. Dai, C. X. Ran, H. Dong, B. Jiao, X. Hou and Z. X. Wu, *ACS Appl. Mater. Inter.*, 2018, **10**, 9849-9857.
86. G. H. Ahmed, J. Yin, R. Bose, L. Sinatra, E. Alarousu, E. Yengel, N. M. AlYami, M. I. Saidaminov, Y. Zhang, M. N. Hedhili, O. M. Bakr, J. L. Bredas and O. F. Mohammed, *Chem. Mater.*, 2017, **29**, 4393-4400.

87. Z. Siddique, J. L. Payne, J. T. S. Irvine, L. K. Jagadamma, Z. Akhter, I. D. W. Samuel and A. Iqbal, *J. Mater. Sci. Mater. El.*, 2020, **31**, 19415-19428.
88. J. Yin, P. Maity, M. De Bastiani, I. Dursun, O. M. Bakr, J. L. Bredas and O. F. Mohammed, *Sci. Adv.*, 2017, **3**.
89. W. Peng, J. Yin, K. T. Ho, O. Ouellette, M. De Bastiani, B. Murali, O. El Tall, C. Shen, X. H. Miao, J. Pan, E. Alarousu, J. H. He, B. S. Ooi, O. F. Mohammed, E. Sargent and O. M. Bakr, *Nano Lett.*, 2017, **17**, 4759-4767.
90. X. Liu, X. Xu, B. Li, Y. Liang, Li, Qi, H. Jiang and D. Xu, *CCS Chemistry*, 2020, **2**, 216-224.
91. H. W. Hu, D. M. Zhao, Y. Gao, X. F. Qiao, T. Salim, B. B. Chen, E. E. M. Chia, A. C. Grimsdale and Y. M. Lam, *Chem. Mater.*, 2019, **31**, 2597-2602.
92. Y. Q. Wang, S. H. Guo, H. Luo, C. K. Zhou, H. R. Lin, X. D. Ma, Q. Y. Hu, M. H. Du, B. W. Ma, W. G. Yang and X. J. Lu, *J. Am. Chem. Soc.*, 2020, **142**, 16001-16006.
93. L. Zhou, J. F. Liao, Z. G. Huang, J. H. Wei, X. D. Wang, H. Y. Chen and D. B. Kuang, *Angew. Chem. Inter. Edit.*, 2019, **58**, 15435-15440.
94. F. Han, W. Y. Yang, H. Li and L. Zhu, *Nanoscale Res. Lett.*, 2020, **15**.
95. Q. Zhou, L. S. Liang, J. J. Hu, B. B. Cao, L. K. Yang, T. J. Wu, X. Li, B. Zhang and P. Gao, *Adv. Energy Mater.*, 2019, **9**.
96. L. L. Mao, Y. L. Wu, C. C. Stoumpos, M. R. Wasielewski and M. G. Kanatzidis, *J. Am. Chem. Soc.*, 2017, **139**, 5210-5215.